

## Full length article

## Input-guidance diffusion model for unknown defect patterns detection in wafer bin map



Seokho Moon, Seoung Bum Kim\*

School of Industrial and Management Engineering, Korea University, Postal Code 02841, Seoul, Republic of Korea

## ARTICLE INFO

**Keywords:**  
 Semiconductor manufacturing  
 Wafer bin map  
 Unknown defect pattern detection  
 Diffusion models

## ABSTRACT

The detection of unknown defect patterns in wafer bin map (WBM) is crucial for maintaining high production yields in semiconductor manufacturing. Existing methods often fail to handle these unknown defect patterns because of their reliance on high-quality labeled data. In this study, we propose a WBM input-guidance diffusion model (WigDM) for detecting unknown defect patterns using unlabeled data. WigDM leverages the specific guidance of input samples to enhance reconstruction quality, allowing effective differentiation between known and unknown patterns. Furthermore, existing unknown detection scores are designed for natural image data and thus fail to accurately reflect the characteristics of WBM. Therefore, the proposed method introduces a new data-driven unknown detection score for WBM dataset. Experimental results on WM-811K and MixedWM38 datasets demonstrate the superiority of the proposed WigDM, outperforming existing methods in 32 out of 36 unknown defect pattern scenarios. The proposed method reduces the reliance on labeled data, offering a new solution for defect pattern detection in semiconductor manufacturing.

## 1. Introduction

The semiconductor industry is a fundamental component of modern technology, playing a crucial role in the production of a wide range of electronic devices. These devices include everyday consumer electronics such as smartphones and laptops, as well as advanced systems used in computing, telecommunications, and industrial applications [1,2]. Many countries consider the semiconductor industry as essential because of its impact on technological innovation and economic growth. With the rapid increase in demand for semiconductors has increased rapidly, the industry must continuously enhance manufacturing processes to boost productivity and meet this growing demand [3].

To achieve this, the semiconductor industry must focus on improving precision and efficiency at every production stage. This includes adopting advanced technologies and rigorous inspection methods to ensure the highest quality [4–7]. Among these, the inspection step is crucial for maintaining high yield rates in increasingly complex production environments. In particular, the electrical die sorting (EDS) process, which uses electronic signals to verify the functionality of the chips on a wafer, is widely used in the inspection process [8]. The results of the EDS process are usually represented in wafer bin maps (WBMs), which visually display the status of each chip as either defective or

functional.

The EDS process can identify the root causes of defects by revealing patterns that indicate specific failures during fabrication [9]. For example, systematic defect patterns in WBMs can highlight recurring issues in certain manufacturing steps, helping engineers trace and fix these problems. Early detection and classification of defects are crucial for maintaining high production yields and ensuring product quality, thus avoiding costly downstream issues.

Traditionally, engineers manually checked the WBMs generated from the EDS process. However, with the increasing complexity of production processes and the growing number of wafers, this task has become increasingly difficult [10]. Moreover, as manufacturing processes become more complicated, the variety of defect patterns in WBMs also increases. This leads to a shortage of skilled engineers capable of accurately identifying these patterns. To address these challenges, research has focused on classifying defect patterns in WBMs using deep learning methods [11–18]. These studies aim to automate the inspection process and improve accuracy. Nonetheless, these methods have a significant limitation: they often fail to handle unknown defect patterns effectively.

Unknown defect patterns refer to data that the deep learning models have not encountered during training step. These models typically

\* Corresponding author.

E-mail addresses: [danny232@korea.ac.kr](mailto:danny232@korea.ac.kr) (S. Moon), [sbkim1@korea.ac.kr](mailto:sbkim1@korea.ac.kr) (S.B. Kim).

struggle to detect such unknown defect patterns, which is critical because these unknown defect patterns can indicate new issues in the manufacturing process. In large-scale semiconductor manufacturing, quickly identifying and addressing the causes of these unknown defect patterns is crucial. Therefore, there is a need for methods that can accurately detect unknown defect patterns. Some research has focused on detecting unknown defect patterns in WBM classification [19–22].

However, most of these studies assume that high-quality labeled data is readily available to build effective defect pattern classifiers. In reality, obtaining high-quality labeled data in WBMs is challenging and time-consuming, often requiring significant resources. Thus, it is necessary to develop methods that can detect unknown defect patterns using only unlabeled data. Out-of-distribution (OOD) detection is a methodology used to identify distributions that were not present in the training set and has been extensively studied in the field of computer vision [23]. Furthermore, OOD detection can be performed even without labels through likelihood-based or reconstruction-based methods. Among these, OOD detection methods based on diffusion models, which have recently shown outstanding performance in many fields, have been proposed [24,25]. However, to the best of our knowledge, no research has applied OOD detection algorithms using diffusion models to WBM data.

In this study, we propose a WBM input-guidance diffusion model (WigDM) for detecting unknown defect patterns. Unlike previous methods that used an unconditional diffusion model, the proposed approach leverages the specific guidance of input samples, addressing the subtle differences between known and unknown defect patterns in WBMs. Additionally, because the method is reconstruction-based, it is crucial to accurately measure the difference between the input image and the reconstructed image. To this end, we use a feature map distance tailored for WBM and propose a data-driven unknown detection score based on the WBM-aware distance. We demonstrate the superiority of the proposed method through various unknown defect patterns scenarios using real WBM datasets, WM-811K [26] and MixedWM38 [27].

The motivation behind WigDM lies in its ability to overcome the limitations of existing WBM classification methods that struggle with unknown defect patterns. Through the application of WBM-specific input guidance, our method addresses the unique challenges posed by the variety and complexity of unknown defect patterns in the semiconductor manufacturing process. Additionally, we aim to provide a more accessible solution by removing the reliance on labeled data, which is often difficult to obtain in this domain. This approach has the potential to significantly enhance the inspection accuracy and efficiency within the semiconductor industry, ensuring robust defect detection without extensive data labeling. The main contributions of this study can be summarized as follows:

- We propose WigDM, a method specifically designed to detect unknown defect patterns in WBM without relying on labeled data. By incorporating WBM-specific input guidance within a denoising diffusion model, our approach improves the performance of unknown defect pattern detection and addresses the challenges posed by the variety and complexity of defects in semiconductor manufacturing.
- We introduce an automated, data-driven unknown detection score that reflects the unique characteristics of WBM, distinguishing them from conventional natural images. This score can automatically determine whether to focus on pixel-level changes or pattern-level changes, enabling more effective detection of unknown defects by adapting to the specific features present in WBM.
- We validate the effectiveness of WigDM through extensive experiments on two publicly available real-world WBM datasets, WM-811K and MixedWM38, demonstrating higher performance across various scenarios. By using publicly open datasets, our proposed method can be readily reproduced, promoting transparency and facilitating further research in this area.

The structure of this paper is organized as follows. Section 2 provides a review of the existing literature on deep learning applications of WBM and OOD detection methods. Section 3 presents the details of our proposed method. In Section 4, we describe the experimental setup and present our results. Finally, Section 5 concludes the paper and offers suggestions for future research.

## 2. Related works

### 2.1. Deep learning applications for wafer bin maps

The EDS process generates WBM data that can be represented as grayscale images. As previously mentioned, defect patterns can be used to identify which manufacturing processes have issues. Expert engineers can associate specific defect patterns with certain process problems. Consequently, most existing research on WBM has focused on defect pattern classification tasks, aiming to improve performance using deep learning techniques. A method using convolutional neural network (CNN) for WBM defect pattern recognition and analysis was proposed, achieving high accuracy in identifying and classifying various defect patterns [11]. A stacking ensemble classifier combining handcrafted features with CNN-extracted features was introduced to enhance WBM defect pattern classification [12]. A mixup-based approach for classifying mixed-type defect patterns in WBM improved performance by generating mixed-type defect patterns during training [13]. A method called SWaCo was proposed for WBM classification using self-supervised contrastive learning to handle unlabeled OOD data, achieving better classification accuracy [14]. A deep CNN model designed for WBM defect identification on imbalanced datasets demonstrated robust performance even with skewed class distributions [15]. Furthermore, generative adversarial network (GAN) has been applied to augment data for minority classes in WBM dataset, which has enhanced the performance of CNN-based defect classification [17]. Similarly, the auxiliary classifier denoising diffusion probabilistic model (ACDDPM) has been proposed to address class imbalance in wafer map defect datasets by generating diverse synthetic samples and combining them with a CNN classifier, significantly improving defect classification accuracy [18].

However, a significant limitation of these traditional studies is their inability to effectively handle unknown defect patterns. The occurrence of unknown defect patterns increases uncertainty in the manufacturing process, posing a significant risk. Therefore, it is crucial to detect these defects quickly in large-scale semiconductor manufacturing processes. To address this issue, several studies have been conducted. For example, a support-weighted ensemble model that combines multiple classifiers to improve the open-set recognition (OSR) of WBM defects was proposed [19]. An optimal bin embedding technique was developed to recognize unknown WBM defect patterns by transforming morphological features of 3D WBM and using simultaneous optimization for better feature vector clustering [20]. Additionally, a decision fusion approach that integrates multiple decision strategies to detect unknown WBM defect patterns was introduced [21]. Finally, a contrastive deep clustering method was presented for detecting new defect patterns in WBM, using contrastive learning to improve the clustering and identification of novel defect patterns [22].

Despite these advancements, such methods still rely on high-quality labeled data to train classifiers. In semiconductor manufacturing, labeling WBMs is a time-consuming process because of the limited availability of expert engineers. Therefore, it is necessary to develop a method that can quickly detect unknown defect patterns using the currently available unlabeled data. Our proposed method addresses this issue by training a diffusion model on unlabeled data and using the reconstruction process to detect unknown defect patterns.

### 2.2. Unsupervised out-of-distribution detection

OOD detection refers to methods that distinguish between a user-

## [Training Step]

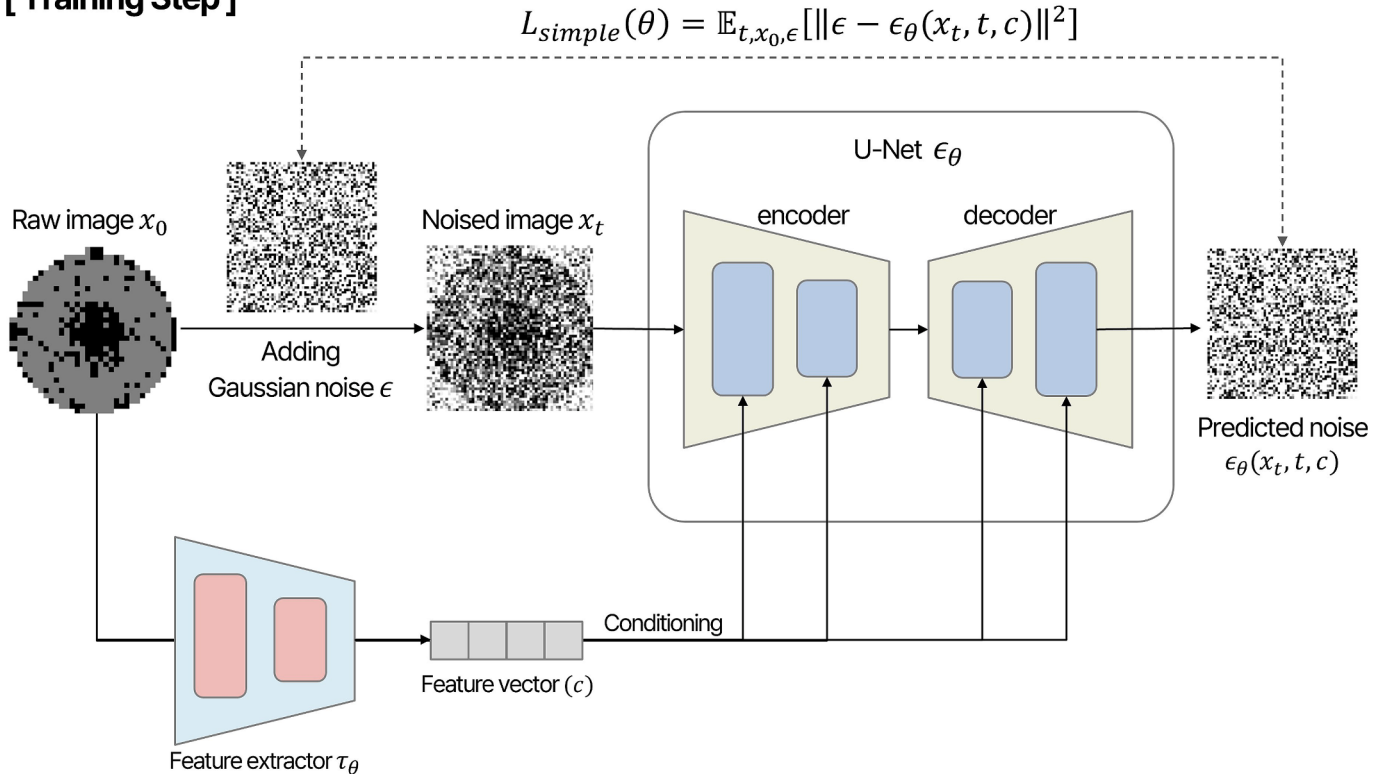


**Fig. 1.** Training step of WigDM. The U-Net model  $\epsilon_\theta$  and feature extractor ResNet-18  $\tau_\theta$  are trained using a known WBM dataset. When Gaussian noise  $\epsilon$  is added to the raw image  $x_0$ , the resulting noised image is denoted as  $x_t$ . The goal of the training is to reduce the difference between the added Gaussian noise  $\epsilon$  and the U-Net's predicted noise  $\epsilon_\theta(x_t, t, c)$ , defined as the  $L_{simple}(\theta)$ . Additionally, the architecture is designed as a conditional diffusion model to effectively convey information from the raw image to the U-Net.

defined in-distribution (ID) dataset and all other datasets, termed OOD. Within this framework, unsupervised OOD detection algorithms, which do not require labeled data, can be primarily categorized into two approaches.

The first approach is likelihood-based. Typically, a generative model, once trained, can compute the likelihood of any given input. The central premise of using likelihood for OOD detection is that samples from the ID dataset will have higher likelihoods, while samples from OOD datasets will exhibit lower likelihoods [28]. Thus, samples with low likelihoods are identified as OOD. However, this approach has demonstrated limitations in certain benchmark datasets, where OOD samples are sometimes assigned high likelihoods [29]. To mitigate this issue, a few studies have been conducted to improve the reliability of likelihood-based methods [30,31]. Despite these efforts, the challenges associated with relying only on likelihood have limited the widespread adoption of this approach.

The second approach is reconstruction-based. The basic assumption is that a model trained on ID samples will reconstruct these samples well, whereas it will struggle with OOD samples. By measuring the distance or error between the input image and the reconstructed image, OOD detection can be performed. Research has used autoencoder models for this purpose, demonstrating that ID samples have lower reconstruction errors compared to OOD samples [32]. Recently, several studies have used diffusion models for reconstruction-based OOD detection because of their effectiveness in image generation. One proposed method involves training a diffusion model on ID samples and generating multiple reconstructed images from the input image with various noise steps. By calculating the error between the input and the reconstructed images, OOD samples can be detected [24]. Another method uses a diffusion model trained on ID data to perform inpainting on masked input images, calculating the error between the input and

reconstructed images for OOD detection [25]. Additionally, a recent study addresses the issue of decreased OOD detection performance due to background similarity between ID and OOD samples by removing background information before reconstruction [33]. However, in WBM datasets, the difference between ID and OOD (in this context, unknown defect patterns) is less clear compared to computer vision benchmark datasets such as MNIST, CIFAR10, and ImageNet. Furthermore, measuring reconstruction error for WBM requires a specialized approach different from that used for natural images. To address these challenges, our study proposes an unknown defect pattern detection framework called WigDM.

### 3. Proposed method

We base our approach on denoising diffusion models for out-of-distribution detection (DDPM-OOD) [24], a high-performing method for OOD detection using diffusion models. The traditional DDPM-OOD trains a diffusion model using a known dataset as the training dataset. During the inference step, various scales of Gaussian noise are injected into the test image, and each noised image is denoised using the trained diffusion model to obtain clean images. Finally, unknown detection is performed by calculating the similarity between the test image and the reconstructed clean images. However, when applied to WBM data, as shown in Fig. 6 for DDPM-OOD, the reconstructed image of a known data sample diverges from the input image as the Gaussian noise step increases. This approach, which judges samples as unknown when their similarity is low, negatively impacts unknown detection performance because the similarity for known samples also decreases. This issue arises easily in WBM datasets in which known and unknown datasets have similar forms, making them difficult to distinguish.

To address this problem, we propose WigDM (WBM input-guidance

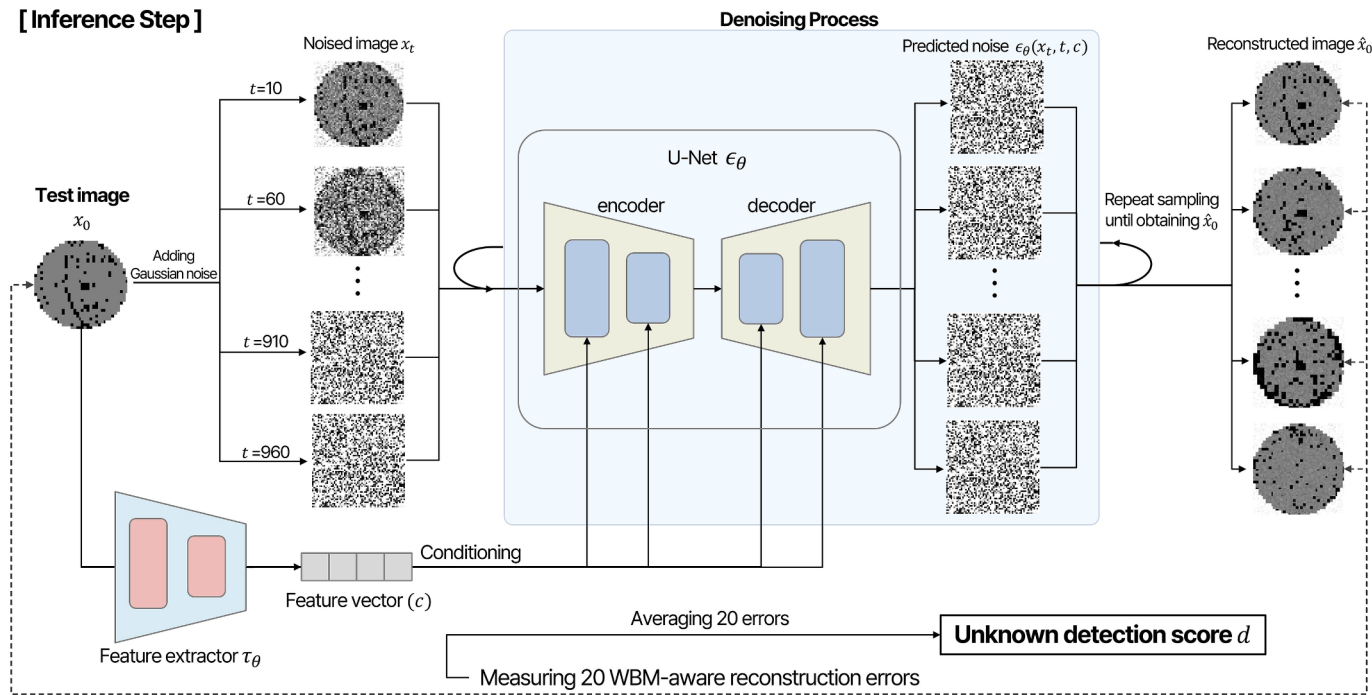


**Fig. 2.** Inference step of WigDM. A test image is perturbed by different levels of noise at various timesteps  $t$ , resulting in the generation of multiple noised images. These images are processed by the trained U-Net model and, after  $t$  iterations, are transformed into the reconstructed images. The reconstruction error between the input image and the reconstructed images is calculated and used for the unknown detection score.

diffusion model) to ensure that the reconstructed image retains the information of the input image even when the Gaussian noise step increases. The proposed model uses a conditional diffusion model structure to incorporate the input image information into the reconstruction process. Conditional diffusion models have recently gained significant attention in the field of generative models. Initially, they were researched for generating images that match user-desired content through text conditioning [34,35]. Recently, methods for incorporating various types of conditioning, including images, have also been studied

[36]. WigDM is the first to use an image conditioning diffusion model structure that uses input image information as guidance for reconstruction, modified for the purpose of unknown detection.

The proposed method is divided into two main steps: the training step and the inference step. First, as shown in Fig. 1, the training of the conditional diffusion model involves adding Gaussian noise to the WBM image  $x_0$  at each timestep  $t$ . The amount of Gaussian noise added follows a user-defined schedule  $\beta_t$ , resulting in the noised image  $x_t$  at timestep  $t$ . This process is known as the forward process or noising process and can

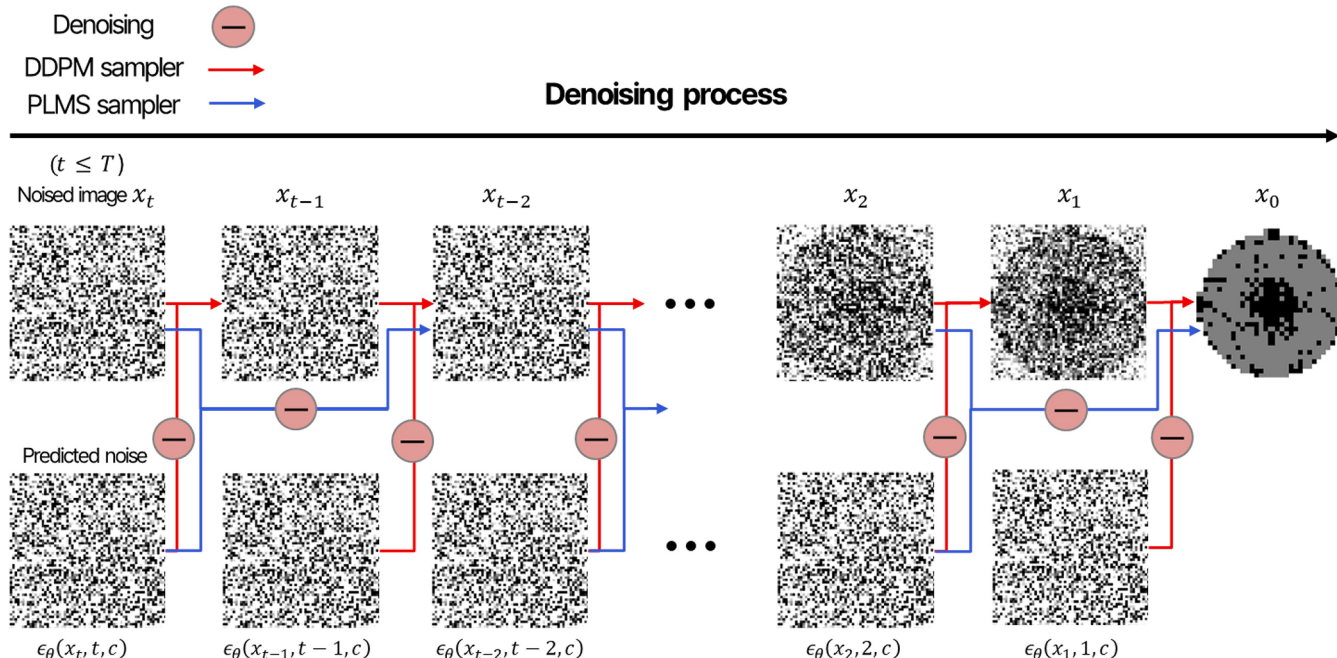


**Fig. 3.** The denoising process compares the DDPM sampler and the PLMS sampler methods. While DDPM sampler passes through all  $t$  steps, PLMS sampler allows skipping a specified number of steps.

be defined as follows:

$$q(x_t|x_0) = N(x_t | \sqrt{\bar{\alpha}_t} x_0, (1 - \bar{\alpha}_t) \mathbf{I}), \# \quad (1)$$

Similar to existing studies,  $0 \leq t \leq T$  and  $\alpha_t := 1 - \beta_t$ , with  $\bar{\alpha}_t := \prod_{s=1}^t \alpha_s$ . It is assumed that  $x_T$  is a completed Gaussian noise image, following the distribution  $X_T \sim \mathcal{N}(0, \mathbf{I})$ . The noise schedule  $\beta_t$  can be set by the user, generally starting small and increasing towards the end. By timestep  $t$ , the fully noised  $x_t$  is considered to have the characteristics of  $x_T \sim \mathcal{N}(0, \mathbf{I})$ .

As suggested in previous research [37], we use loss function  $L_{\text{simple}}(\theta)$ , which can be represented by the difference between the noise value given to the input image and the noise value predicted by the model, as follows:

$$L_{\text{simple}}(\theta) = \mathbb{E}_{t, x_0, \epsilon} \left[ \|\epsilon - \epsilon_\theta(x_t, t, c)\|^2 \right], \# \quad (2)$$

where  $c$  denotes the feature vector from feature extractor ResNet-18  $\tau_\theta$ .  $(x_t, t, c)$  represents the inputs to the U-Net  $\epsilon_\theta$ . And  $\epsilon_\theta(x_t, t, c)$  represents a predicted Gaussian noise image. After training the model with known WBM dataset, we can define the reverse process (or denoising process), which aims to estimate probability of  $x_{t-1}$  given  $x_t$ . To generate clean images, we use the Gaussian transition representing the relationship between timestep  $t-1$  and  $t$  during the denoising process. An image at timestep  $t-1$  can be generated from an image at timestep  $t$  as follows:

$$x_{t-1} = \frac{1}{\sqrt{\alpha_t}} \left( x_t - \frac{1 - \alpha_t}{\sqrt{1 - \bar{\alpha}_t}} \epsilon_\theta(x_t, t, c) \right) + \sigma_t z, \# \quad (3)$$

where  $x_T \sim \mathcal{N}(0, \mathbf{I})$  and  $z \sim \mathcal{N}(0, \mathbf{I})$  if  $t > 1$ , else  $z = 0$ . This process is repeated until the fully clean image  $x_0$  is obtained. Additionally, the denoising process can be initiated from any  $x_t$  (for  $t < T$ ). In other words, the diffusion model can perform denoising on  $x_t$  injected with noise at any scale, leveraging this property to reconstruct images during the inference step.

As shown in Fig. 2, the inference step uses the trained model, subjecting the test image to noised steps at  $t = 10, 60, \dots, 910, 960$ , creating a total of 20 noised images. The trained model then denoises these 20 noised images. Introducing varying levels of noise into the input data and performing denoising is essential because it is uncertain at which noise level the information within the input data becomes fully degraded. By injecting noise of various scales and averaging the reconstructed images, the model captures the distinctive contributions of different scales without biasing toward any specific scale. This averaging approach enhances the robustness of the model in detecting unknown defect patterns by leveraging the varying degrees of information preservation across different noise levels. The denoising process using the diffusion model, also referred to as sampling, involves removing the predicted noise from the noised image step by step to obtain the final clean image, as illustrated in Fig. 3. In this study, we use the pseudo-likelihood maximization sampler (PLMS) sampler, which is faster than the DDPM sampler. Naturally, the larger the noise step, the longer the denoising process. This process is repeated until a clean reconstruction image is obtained.

This results in a total of 20 reconstructed images, which are then used to calculate the reconstruction error with the test image, forming the final unknown detection score. However, existing approaches that use learned perceptual image patch similarity (LPIPS) [38] to measure the reconstruction error between the input image and the unknown image do not effectively capture the characteristics of WBM. This is because WBM images, consisting of black patterns on a gray background, are significantly different from real-world data. To address these issues, the proposed WigDM defines a data-driven unknown detection score. The detailed method for calculating the unknown detection score is described in Section 4.2. In summary, by calculating the unknown detection score through the training step and inference

**Table 1**

The number of data points during training, validation, and inference steps.

Defect pattern	All	Train	Valid	inference (when each pattern is treated as unknown)
Center (C)	4,294	3,865	429	1,000
Donut (D)	555	500	55	555
Edge-loc (EL)	5,189	4,671	518	1,000
Edge-ring (ER)	9,680	8,712	968	1,000
Loc (L)	3,593	3,234	359	1,000
Scratch (S)	1,193	1,074	119	1,000
Near-full (NF)	149	135	14	149
C + EL	1,000	0	0	1,000
C + ER	1,000	0	0	1,000
C + L	1,000	0	0	1,000
C + S	1,000	0	0	1,000
D + EL	1,000	0	0	1,000
D + ER	1,000	0	0	1,000
D + L	1,000	0	0	1,000
D + S	1,000	0	0	1,000
EL + L	1,000	0	0	1,000
EL + S	1,000	0	0	1,000
ER + L	1,000	0	0	1,000
ER + S	1,000	0	0	1,000
L + S	1,000	0	0	1,000
C + EL + L	1,000	0	0	1,000
C + EL + S	2,000	0	0	1,000
C + ER + L	1,000	0	0	1,000
C + ER + S	1,000	0	0	1,000
C + L + S	1,000	0	0	1,000
D + EL + L	1,000	0	0	1,000
D + EL + S	1,000	0	0	1,000
D + ER + L	1,000	0	0	1,000
D + ER + S	1,000	0	0	1,000
D + L + S	1,000	0	0	1,000
EL + L + S	1,000	0	0	1,000
ER + L + S	1,000	0	0	1,000
C + EL + L + S	1,000	0	0	1,000
C + ER + L + S	1,000	0	0	1,000
D + EL + L + S	1,000	0	0	1,000
D + ER + L + S	1,000	0	0	1,000

steps, we can detect unknown WBM defect patterns.

## 4. Experiment

### 4.1. Data

In this study, we used two WBM datasets collected from actual manufacturing processes: WM-811K and MixedWM38. The WM-811K dataset comprises a total of 811,457 samples, out of which 172,950 samples are labeled by experts into nine classes. To construct scenarios with various classes of unknown defect patterns, we used only the labeled data as shown in Table 1. Additionally, the “none” class was excluded because it does not represent a defect pattern, and the “random” class was excluded because of its similarity to the “near-full” class. Consequently, the seven classes used in this experiment are “center”, “donut”, “edge-loc”, “edge-ring”, “loc”, “scratch”, and “near-full”. The MixedWM38 dataset consists of 38,015 instances, labeled into 38 single and mixed defect pattern classes. We used a total of 29 classes of mixed defect patterns to construct various scenarios of unknown defect patterns. These patterns are grouped based on the number of combined defects as follows:

- 2 mixed-type defect Patterns (13 classes): “C + EL (center + edge-loc)”, “C + ER (center + edge-ring)”, “C + L (center + loc)”, “C + S (center + scratch)”, “D + EL (donut + edge-loc)”, “D + ER (donut + edge-ring)”, “D + L (donut + loc)”, “D + S (donut + scratch)”, “EL + L (edge-loc + loc)”, “EL + S (edge-loc + scratch)”, “ER + L (edge-ring + loc)”, “ER + S (edge-ring + scratch)”, “L + S (loc + scratch)”
- 3 mixed-type defect patterns (12 classes): “C + EL + L (center + edge-loc + loc)”, “C + EL + S (center + edge-loc + scratch)”, “C + ER

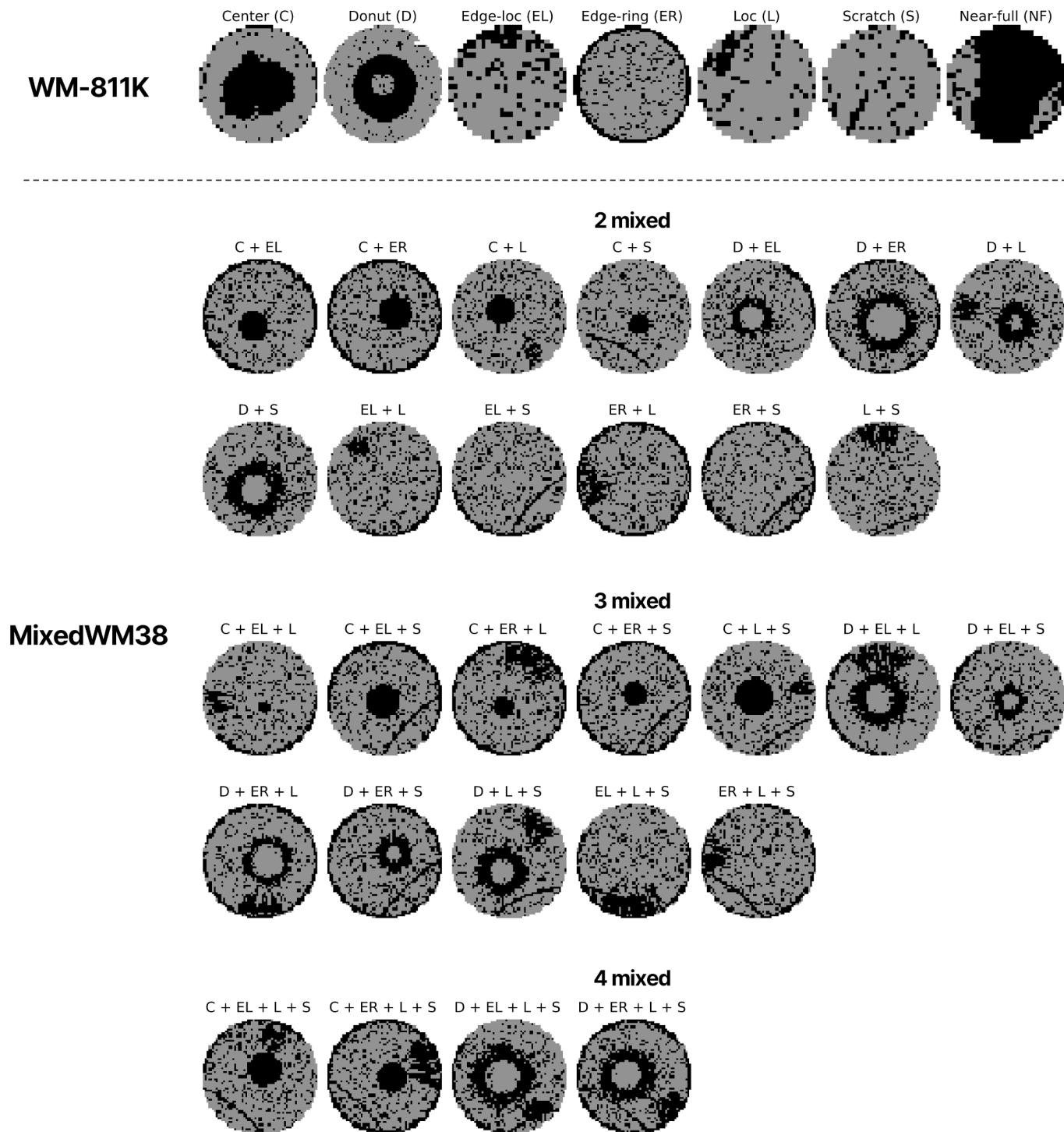
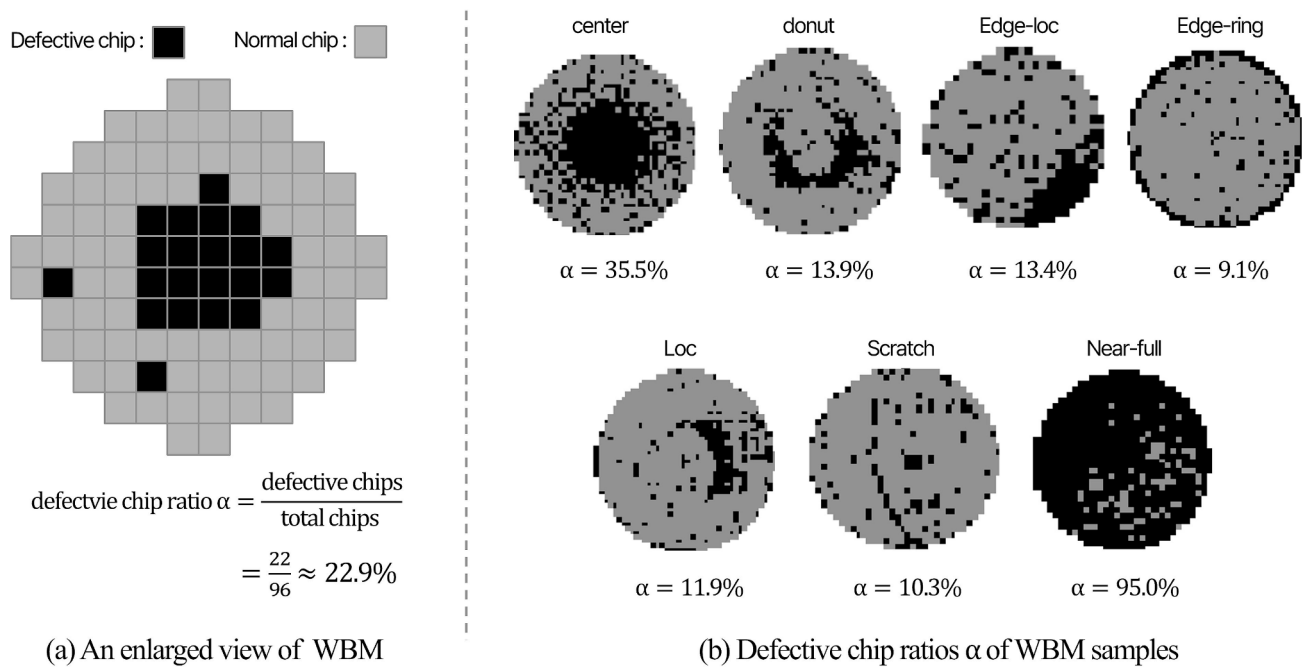


**Fig. 4.** Visualization of all defect pattern images used for experiments from the WM-811 K and MixedWM38 datasets.

- + L (center + edge-ring + loc)", "C + ER + S (center + edge-ring + scratch)", "C + L + S (center + loc + scratch)", "D + EL + L (donut + edge-loc + loc)", "D + EL + S (donut + edge-loc + scratch)", "D + ER + L (donut + edge-ring + loc)", "D + ER + S (donut + edge-ring + scratch)", "D + L + S (donut + loc + scratch)", "EL + L + S (edge-loc + loc + scratch)", "ER + L + S (edge-ring + loc + scratch)"
- 4 mixed-type defect patterns (4 classes): "C + EL + L + S (center + edge-loc + loc + scratch)", "C + ER + L + S (center + edge-ring + loc + scratch)", "D + EL + L + S (donut + edge-loc + loc + scratch)", "D + ER + L + S (donut + edge-ring + loc + scratch)"

**Fig. 4** shows the images of the defect patterns used from both datasets. WBMs are collected in various sizes, but for the convenience of model training, they were resized to 64x64 and converted to 1-channel grayscale images.

When constructing training datasets for each scenario, as shown in **Table 1**, 90 % of the data from each defect pattern class was used for training, and the remaining 10 % was used for validation. For instance, in Scenario 1, "donut," "edge-loc," "edge-ring," "loc," "scratch" and "near-full" were taken from the WM-811 K dataset, with 90 % used for training. The model was then evaluated on its ability to detect the "center" unknown defect pattern. The number of instances for each



(a) An enlarged view of WBM

(b) Defective chip ratios  $\alpha$  of WBM samples

**Fig. 5.** (a) An enlarged view of WBM illustrating calculation of defective chip ratio  $\alpha$  through an example. (b) Results of calculating defective chip ratio  $\alpha$  for seven examples of WBM.

dataset was listed in Table 1. For the unknown defect pattern data, 1,000 samples were selected from each defect pattern class. If a class contained more than 1,000 samples, 1,000 were randomly selected, and if it contained fewer than 1,000 samples, all available samples were used.

#### 4.2. Experimental setting

To demonstrate the effectiveness of the proposed method, we compared with the following six existing unsupervised OOD detection methods:

1. Likelihood: unknown detection based on  $p(\mathbf{x}; \theta)$  obtained from a generative model. The generative model used here is a diffusion model [28].

2. Anomaly detection with generative adversarial networks (AnoGAN): A generative adversarial network composed of a generator and a discriminator is trained. unknown detection is performed based on the weighted sum of residual loss and discrimination loss:  $\lambda \bullet |x - G(z_\gamma)| + (1 - \lambda) \bullet |f(x) - f(G(z_\gamma))|$  where  $f(\bullet)$  is the discriminator's feature extractor,  $G(\bullet)$  is the generator,  $z_\gamma$  is random noise, and  $\lambda$  is set to 0.9 [39].
3. Autoencoder: A three-layer autoencoder is trained. During inference, the mean squared error (MSE)  $\|x - \hat{x}\|_2$  is measured between the input image and the reconstructed image. MSE is used for unknown detection.
4. Memory-augmented deep autoencoder (MemAE): An autoencoder with a memory bank designed to retain more information from the

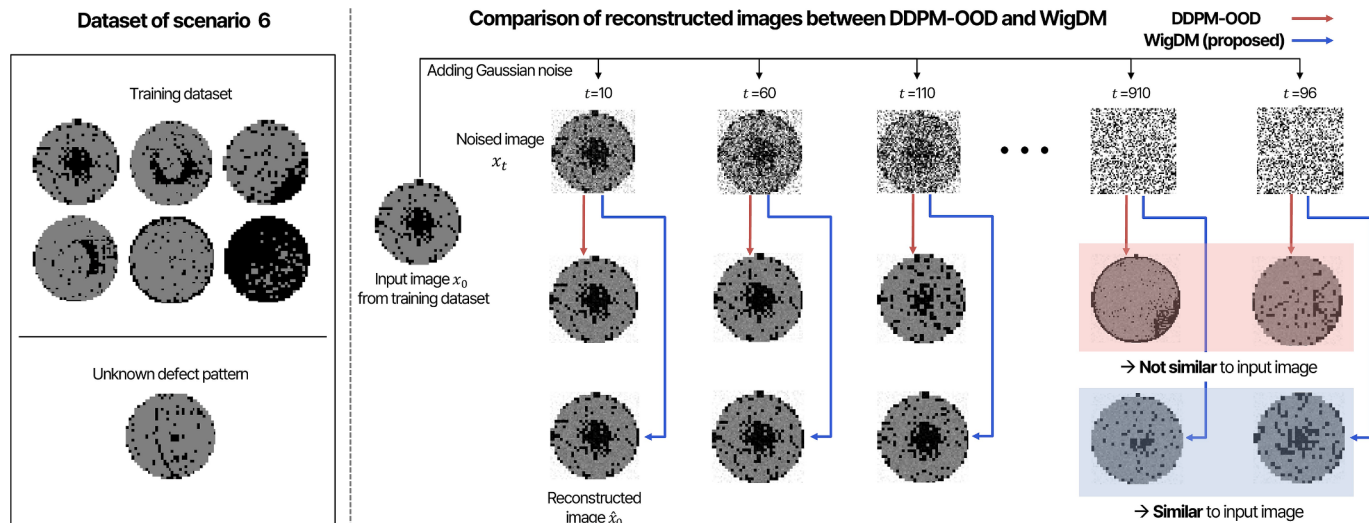


**Fig. 6.** Comparison of reconstructed image results between DDPM-OOD and WigDM. DDPM-OOD, without input guidance, produces reconstructed images that are not similar to the input image when  $t$  is high for noised images. In contrast, the proposed WigDM, through input guidance, ensures similarity to the input image even at high  $t$  for noised images.

**Table 2**

AUROC performance for unknown defect pattern detection across 36 scenarios comparing the proposed WigDM with six other methods. Scenarios 1 to 7 focus on the detection of single-type defect patterns; Scenarios 8 to 20 focus on the detection of 2 mixed-type defect patterns; Scenarios 21 to 32 address the detection of 3 mixed-type defect patterns; and Scenarios 33 to 36 focus on the detection of 4 mixed-type defect patterns. The best performance is highlighted in bold, and the second-best performance is underlined.

No.	Training dataset	Unknown defect pattern	Likelihood	Ano GAN	Autoencoder	MemAE	LMD	DDPM-OOD	WigDM (Proposed)
1	D, EL, ER, L, S, NF	Center (C)	0.493	<u>0.631</u>	0.625	0.630	0.539	<b>0.665</b>	0.619
2	C, EL, ER, L, S, NF	Donut (D)	0.716	<u>0.704</u>	0.730	0.759	0.674	<u>0.865</u>	<b>0.908</b>
3	C, D, ER, L, S, NF	Edge-loc (BL)	0.520	0.593	0.550	0.633	<u>0.680</u>	0.623	<b>0.793</b>
4	C, D, EL, L, S, NF	Edge-ring (ER)	0.801	0.749	0.788	0.778	0.538	<u>0.806</u>	<b>0.900</b>
5	C, D, EL, ER, S, NF	Loc (L)	0.452	0.465	0.424	0.558	<u>0.755</u>	0.625	<b>0.857</b>
6	C, D, EL, ER, L, NF	Scratch (S)	0.409	0.350	0.560	0.506	<u>0.742</u>	0.447	<b>0.846</b>
7	C, D, EL, ER, L, S	Near-full (NF)	0.920	0.939	0.647	0.640	0.768	<u>0.986</u>	<b>0.992</b>
8	D, ER, L, S, NF	C + EL	<u>0.996</u>	0.934	0.896	0.880	0.841	0.992	<b>0.997</b>
9	D, ER, L, S, NF	C + ER	0.994	0.980	0.901	0.916	0.830	<u>0.996</u>	<b>0.998</b>
10	D, EL, ER, S, NF	C + L	<u>0.995</u>	0.940	0.898	0.947	0.968	<b>0.998</b>	0.998
11	D, EL, ER, L, NF	C + S	0.967	0.942	0.937	0.860	0.951	<u>0.995</u>	<b>0.997</b>
12	C, ER, L, S, NF	D + EL	<u>0.997</u>	0.917	0.864	0.856	0.912	<b>0.999</b>	0.999
13	C, EL, L, S, NF	D + ER	<u>0.992</u>	0.955	0.903	0.899	0.925	<b>0.999</b>	0.999
14	C, EL, ER, S, NF	D + L	<u>0.990</u>	0.949	0.879	0.901	0.930	<b>1.000</b>	1.000
15	C, EL, ER, L, NF	D + S	<u>0.991</u>	0.960	0.882	0.933	0.929	<b>1.000</b>	1.000
16	C, D, ER, S, NF	EL + L	0.983	0.918	0.907	0.909	0.907	<u>0.995</u>	<b>0.998</b>
17	C, D, ER, L, NF	EL + S	0.984	0.963	0.922	0.917	0.867	<u>0.998</u>	0.996
18	C, D, EL, S, NF	ER + L	0.991	0.976	0.891	0.883	0.881	<u>0.995</u>	<b>0.998</b>
19	C, D, EL, L, NF	ER + S	0.985	0.929	0.920	0.921	0.879	<b>0.998</b>	<u>0.996</u>
20	C, D, EL, ER, NF	L + S	0.995	0.941	0.876	0.903	0.866	<u>0.999</u>	<b>1.000</b>
21	D, ER, S, NF	C + EL + L	0.961	0.923	0.850	0.879	0.918	<u>0.972</u>	0.982
22	D, ER, L, NF	C + EL + S	0.940	0.919	0.901	0.922	0.910	<u>0.959</u>	0.988
23	D, EL, S, NF	C + ER + L	0.933	0.938	0.899	0.920	0.922	<u>0.956</u>	<b>0.989</b>
24	D, EL, L, NF	C + ER + S	0.958	0.936	0.870	0.887	0.943	<u>0.962</u>	<b>0.991</b>
25	D, EL, ER, NF	C + L + S	<u>0.994</u>	0.956	0.967	0.985	0.980	<b>1.000</b>	1.000
26	C, ER, S, NF	D + EL + L	0.937	0.949	0.873	0.889	0.956	<u>0.962</u>	0.994
27	C, ER, L, NF	D + EL + S	0.921	0.902	0.897	0.908	0.944	<u>0.977</u>	0.995
28	C, EL, S, NF	D + ER + L	0.918	0.900	0.915	0.877	0.938	<u>0.962</u>	0.996
29	C, EL, L, NF	D + ER + S	<u>0.970</u>	0.943	0.895	0.926	0.940	0.966	0.988
30	C, EL, ER, NF	D + L + S	0.948	0.912	0.924	0.930	0.927	<u>0.968</u>	0.998
31	C, D, ER, NF	EL + L + S	0.956	0.902	0.937	0.923	0.885	<u>0.981</u>	0.989
32	C, D, EL, NF	ER + L + S	0.949	0.933	0.860	0.874	0.931	<u>0.955</u>	0.991
33	D, ER, NF	C + EL + L + S	0.908	0.869	0.881	0.878	0.904	0.927	0.945
34	D, EL, NF	C + ER + L + S	0.907	0.885	0.905	0.911	0.899	<b>0.921</b>	0.915
35	C, ER, NF	D + EL + L + S	0.928	0.903	0.912	0.918	0.937	<u>0.955</u>	<b>0.961</b>
36	C, EL, NF	D + ER + L + S	0.916	0.894	0.923	0.910	0.958	<u>0.950</u>	<b>0.964</b>
Average AUROC			0.895	0.872	0.845	0.855	0.869	<u>0.926</u>	<b>0.960</b>

training dataset, enhancing detection performance. MSE is used as the criterion [32].

5. Lift, map, detect (LMD): Leveraging the capability of a trained diffusion model to perform inpainting on masked images, reconstruction of the masked input image is performed during inference. unknown detection is based on the LPIPS value between the input image and the reconstructed image [25].
6. DDPM-OOD: Using the ability of diffusion models to denoise Gaussian noise at various steps. In inference step, Gaussian noise is added to the input image at multiple levels, and denoising is conducted. The MSE and LPIPS values between the input and reconstructed images are normalized using Z-scores and summed for unknown detection [24].

The proposed method adopted a standard architecture commonly used in diffusion model research [40]. This architecture consisted of a three-layer U-Net with channel dimensions of [256, 512, 784]. To integrate the condition into the U-Net, we used a ResNet-18 structure as the feature extractor for the input image [41]. This condition was incorporated into every block of the U-Net through attention operations. Additionally, the time step value of the Gaussian noise was embedded into a 1024-dimensional vector using a multi-layer perceptron. The optimizer used for training was adaptive moment estimation (Adam) [42] with a learning rate of 0.00001. All datasets were trained for 500 epochs, with a noise scheduling of beta values between 0.0015 and 0.0195, similar to typical diffusion models [24,43]. The batch size was

set to 512, and training was conducted on a single NVIDIA A100 GPU with 80 GB memory. During inference, as described in Section 3, the PLMS sampler was used to reduce the 1000-step generation process of the DDPM sampler to 25 steps for reconstruction.

As previously mentioned, traditional unknown detection scores were not suitable for WBM. Metrics like LPIPS, trained on natural images, or simple pixel-wise differences like MSE, did not effectively capture the differences between the input and reconstructed WBM data. Therefore, we proposed an unknown detection score  $d$  that simultaneously captured pixel-level changes and WBM-specific pattern changes, defined as follows:

$$d = \sum_{n=1}^{20} \alpha \bullet \text{Recon}_{\text{pixel}}(x_0, \hat{x}_{0,n}) + (1 - \alpha) \bullet \text{Recon}_{\text{WBM-patterns}}(x_0, \hat{x}_{0,n}), \# \quad (4)$$

where  $\alpha$  is the defective chip ratio of a single wafer, as shown in Fig. 5.  $x_0$  represents the input image, while  $\hat{x}_{0,n}$  denotes each image of reconstructed images generated according to the noise scale, as illustrated in Fig. 2. The errors between the input image and the reconstructed image,  $\text{Recon}_{\text{pixel}}$  and  $\text{Recon}_{\text{WBM-patterns}}$ , are defined as follows.

$$\text{Recon}_{\text{pixel}}(x, \hat{x}) = \|x - \hat{x}\|_2, \# \quad (5)$$

$$\text{Recon}_{\text{WBM-patterns}}(x, \hat{x}) = \sum_{l=1}^{H_l} \sum_{w=1}^{W_l} \|w^l \odot (m_{hw}^l - \hat{m}_{hw}^l)\|_2^2, \# \quad (6)$$

where  $m$  denotes the feature maps of image  $x$  in the ResNet-18 archi-

ture, obtained through a self-supervised learning approach [44]. Here,  $h$  and  $w$  denote the height and width of the feature map, respectively, and  $l$  represents each layer of the ResNet-18 in which  $w^l$  corresponds to the weights of each layer. In this experiment, we treated all  $w^l$  as one.

The use of a data-driven  $\alpha$  was motivated by the need for a score that reflected the characteristics of the input WBM. For instance, detecting patterns like “near-full” required a higher weight for  $Recon_{pixel}$  because of the significance of pixel-level changes. Conversely, for defect patterns like “scratch” or “edge-loc,” the detection relied more on the pattern changes between the input and reconstructed images, necessitating a higher weight for  $Recon_{WBM-patterns}$ . To avoid the need for manual weight selection by the user, we used the defective chip ratio  $\alpha$  of the input image, as shown in Fig. 5, to determine the weights automatically. To explain in detail, Fig. 5 (a) shows an enlarged view of WBM, which indicates that the WBM consists of multiple defective chips combined with normal chips.

Additionally, by leveraging the binary data characteristics of the WBM, the ratio of defective chips in a single wafer can be calculated. This can be performed by dividing the number of defective chips by the total number of chips. Fig. 5 (b) presents the defect chip ratios  $\alpha$  calculated for seven different WBM defect pattern samples. As mentioned before, in the case of “scratch” or “edge-loc” defect patterns,  $\alpha$  values are small, which automatically gives a higher weight to  $Recon_{WBM-patterns}$  according to equation (4).

#### 4.3. Results

As shown in Table 2, we evaluated unknown defect pattern detection across 36 scenarios using the area under the receiver operating characteristic (AUROC), a standard metric in out-of-distribution and anomaly detection tasks where values closer to one indicate better performance. The proposed method, WigDM, achieved superior performance in 32 out of 36 scenarios, with an average AUROC of 0.960, significantly higher than the next-best method, DDPM-OOD, which had an average AUROC of 0.926. Particularly in challenging scenarios involving difficult-to-detect defect patterns such as “edge-loc,” “loc,” and “scratch,” WigDM outperformed existing methods, highlighting its practical relevance in real-world applications.

In Scenarios 1 to 7, which involve single defect patterns as unknowns, WigDM showed remarkable performance, particularly in scenarios where other methods struggled. For instance, in Scenario 3 (“edge-loc”), WigDM achieved an AUROC of 0.793, while other methods like Likelihood and Autoencoder scored 0.520 and 0.550, respectively. This indicates a substantial improvement in detecting the “edge-loc” defect, which is often challenging because of its subtle features and similarity to other patterns. Similarly, in Scenario 5 (“loc”), WigDM achieved an AUROC of 0.857, significantly outperforming the other methods, with the highest AUROC among them being 0.755 by LMD. In Scenario 6 (“scratch”), WigDM achieved an AUROC of 0.846, while the other methods had considerably lower scores, with Likelihood at 0.409 and DDPM-OOD at 0.447. These results highlight WigDM’s effectiveness in detecting difficult defect patterns, demonstrating its practical relevance in real-world applications where such defects may have significant implications for product quality.

In Scenarios 8 to 20, which focus on 2 mixed-type defect patterns common in practical settings because of the complexity of manufacturing processes, WigDM consistently yielded superior performance. For example, in Scenarios 14 and 15, WigDM achieved perfect AUROC scores of 1.000 in detecting “D + L” and “D + S” defect patterns. In Scenarios 8 to 20, WigDM’s AUROC scores ranged from 0.996 to 1.000, consistently outperforming other methods that showed more variability in their performance. This consistent high performance suggests that WigDM is robust in handling the increased complexity introduced by mixed defect patterns, effectively capturing the nuances that

**Table 3**

AUROC performance of WigDM on non-mixed unknown defect pattern scenarios using MSE, LPIPS, and proposed unknown detection score  $d$ . The best performance is highlighted in bold.

No.	Training dataset	Unknown defect pattern	MSE	LPIPS	$d$ (unknown detection score)
1	D, EL, ER, L, S, NF	Center (C)	0.557	<b>0.623</b>	0.619
2	C, EL, ER, L, S, NF	Donut (D)	0.725	0.740	<b>0.908</b>
3	C, D, ER, L, S, NF	Edge-loc (EL)	0.460	0.656	<b>0.793</b>
4	C, D, EL, L, S, NF	Edge-ring (ER)	0.541	0.688	<b>0.900</b>
5	C, D, EL, ER, S, NF	Loc (L)	0.359	0.747	<b>0.857</b>
6	C, D, EL, ER, L, NF	Scratch (S)	0.236	0.820	<b>0.846</b>
7	C, D, EL, ER, L, S	Near-full (NF)	0.955	0.853	<b>0.992</b>

arise when multiple defects occur simultaneously.

Moreover, in Scenarios 21 to 32, involving 3 mixed-type defect patterns, and Scenarios 33 to 36, involving 4 mixed-type defect patterns, WigDM continued to outperform other methods. In Scenarios 25, WigDM achieved perfect AUROC scores of 1.000, demonstrating its ability to detect even highly complex defect combinations. In the most complex scenarios involving mixed defect patterns, such as Scenarios 33, 35, and 36, WigDM consistently achieved the highest AUROC scores, ranging from 0.945 to 0.964. For example, in Scenario 33, WigDM scored 0.945, outperforming DDPM-OOD, which scored 0.927. Similarly, in Scenario 36, WigDM achieved 0.964 compared to DDPM-OOD’s 0.950. However, in Scenario 34, WigDM’s AUROC of 0.915 was slightly below DDPM-OOD’s score of 0.921. These results highlight WigDM’s ability to maintain high detection performance even in challenging scenarios with multiple mixed-type patterns. This strength demonstrates WigDM’s effectiveness in handling complex defect distributions, making it a reliable choice for real-world applications.

As shown in Table 3, we demonstrated the superiority of our proposed unknown detection score  $d$  compared to traditional metrics like MSE and LPIPS. While MSE or LPIPS performed better depending on the defect pattern, our proposed  $d$  calculated the score in a data-driven manner based on the input image. Additionally, by using a feature map distance specifically modified for WBM, our method achieved superior performance across various defect patterns. Additionally, as mentioned in Equation (6), we used a feature map distance specifically modified for WBM. Here,  $m$  denotes the feature maps from a ResNet-18 architecture that was separately trained using a self-supervised learning method [44] on the WM-811K dataset, allowing our method to achieve superior performance across various defect patterns.

The reasons for the superior performance of the proposed method are illustrated in Fig. 6. In this example, the dataset setting of Scenario 6 was used, with detailed information presented on the left side of Fig. 6. Specifically, both DDPM-OOD and WigDM were trained using the training dataset from Scenario 6. The red line represents the denoising process of the conventional DDPM-OOD, while the blue line depicts the denoising process of WigDM. Typically, as the noise step increases and  $t$  grows larger, the information from the input image tends to be lost, leading to a higher probability of randomly reconstructing one of the images from the training dataset. Therefore, the DDPM-OOD often reconstructs patterns that differ from the input image but match one from the training set. To address this issue, WigDM, which uses an input-guidance diffusion model, maintains an image similar to the input image even at noise steps as high as 990. In addition, because the unknown detection score is based on the pixel and pattern changes between the input image and the reconstructed image, the score remains low, allowing the data to be classified as a known defect pattern. This

**Table 4**

Inference time per wafer, maximum number of manufactured wafers per day, and total inference time per day across seven methods.

	Likelihood	Ano GAN	Autoencoder	MemAE	LMD	DDPM-OOD	WigDM (Proposed)
Inference time / wafer (seconds)	11.7	3.5	1.0	1.3	13.9	13.1	14.3
Maximum number of manufactured wafers / day	1000	1000	1000	1000	1000	1000	1000
Total inference time / day (hours)	3.25	0.97	0.28	0.36	3.86	3.64	3.97

robust performance is attributed to WigDM's ability to effectively preserve the input image characteristics throughout the denoising process, which is particularly crucial for accurate unknown defect pattern detection in complex and mixed defect pattern scenarios.

As shown in Table 4, the inference times for likelihood, LMD, DDPM-OOD, and WigDM, which are based on diffusion models, were longer than those for AnoGAN, autoencoder, and MemAE. However, considering that the maximum number of wafers producible in a semiconductor manufacturing line is 1000 per day, the total inference time per day for WigDM was 3.97 h, assuming 1000 wafers were produced each day. Therefore, although the inference time was longer compared to other models, it was feasible to inspect the entire daily production of wafers in a practical setting. Hence, applying the highest-performing WigDM could effectively replace the manual labor of engineers.

## 5. Conclusion

In this study, we present WigDM, a conditional diffusion model for detecting unknown defect patterns in WBM without the need for labeled data. Our approach integrates WBM-specific input guidance into the denoising process, allowing the model to preserve the characteristics of the input image while effectively differentiating between known and unknown patterns. Experimental results on WM-811 K and MixedWM38 datasets confirm the robustness and superiority of WigDM across multiple scenarios. By reducing the dependence on labeled data, WigDM addresses a significant challenge in the field.

Despite its superior performance, WigDM has several limitations. One drawback is the high training cost associated with diffusion models compared to other CNN-based models, necessitating careful calculation of economic benefits and costs for practical applications. Additionally, because of the nature of diffusion models, the inference process involves time-consuming denoising through predicted noise. Although this study uses the PLMS sampler to reduce inference time, it remains a challenging issue. Nevertheless, as mentioned in Section 4.3, it is feasible to inspect all wafers produced in actual semiconductor manufacturing processes within a reasonable amount of time. Recently, a one-step generation diffusion model known as the consistency model [45] has been studied. Future research should focus on applying this method to further reduce inference time. In addition, future research will explore the potential of integrating semi-supervised learning techniques, such as active learning into our framework. While our current method operates in a fully unsupervised setting, the inclusion of a small amount of labeled data through active learning could improve detection performance and facilitate more efficient labeling, particularly for challenging defect patterns. Moreover, we plan to improve the model by including visually indistinguishable samples, such as the random class, to evaluate its performance in more complex and realistic scenarios. This expansion aims to further enhance the applicability and effectiveness of WigDM in diverse real-world conditions.

## CRediT authorship contribution statement

**Seokho Moon:** Writing – original draft, Visualization, Software, Methodology, Investigation, Formal analysis, Data curation, Conceptualization. **Seoung Bum Kim:** Writing – review & editing, Validation,

Supervision, Resources, Project administration, Funding acquisition.

## Funding

This research was supported by Brain Korea 21 FOUR, the Ministry of Science and ICT (MSIT) in Korea under the ITRC support program supervised by the Institute for Information Communication Technology Planning and Evaluation (IITP-2020-0-01749), the National Research Foundation of Korea grant funded by the Korea government (RS-2022-00144190), Culture, Sports and Tourism R&D Program through the Korea Creative Content Agency grant funded by the Ministry of Culture, Sports and Tourism in 2024 (Project Name: Development of AI-based large-scale automatic game verification technology to improve game production verification efficiency for small and medium-sized game companies, Project Number: RS-2024-00393500, Contribution Rate: 100%), and Korea Planning & Evaluation Institute of Industrial Technology (RS-2024-00426183).

## Declaration of competing interest

The authors declare that they have no known competing financial interests or personal relationships that could have appeared to influence the work reported in this paper.

## Acknowledgments

The authors would like to express their sincere gratitude to the editor and anonymous reviewers for their valuable feedback and constructive suggestions, which have significantly contributed to improving the quality and clarity of this manuscript. Their thoughtful comments and recommendations were instrumental in refining our analysis and presentation.

## Data availability

All research data are publicly available at: <https://www.kaggle.com/datasets/qingyi/wm811k-wafer-map>, <https://www.kaggle.com/datasets/co1d7era/mixedtype-wafer-defect-datasets>.

## References

- [1] H. Casper, A. Rexford, D. Riegel, A. Robinson, E. Martin, M. Awwad, The impact of the computer chip supply shortage, in: Proceedings of the international conference on industrial engineering and operations management, Bangalore, India, 2021, pp. 236–245.
- [2] R. Nikandish, E. Blokhina, D. Leipold, R.B. Staszewski, Semiconductor quantum computing: toward a CMOS quantum computer on chip, *IEEE Nanotechnol. Mag.* 15 (6) (2021) 8–20.
- [3] J. Shim, S. Cho, E. Kum, S. Jeong, Adaptive fault detection framework for recipe transition in semiconductor manufacturing, *Comput. Ind. Eng.* 161 (Nov. 2021), <https://doi.org/10.1016/j.cie.2021.107632>.
- [4] H. Chun, J. Wang, J. Kim, C. Lee, Wafer particle inspection technique using computer vision based on a color space transform model, *Int. J. Adv. Manuf. Technol.* 127 (11–12) (2023) 5063–5071.
- [5] J. Yu, S. Han, C.-O. Lee, Defect inspection in semiconductor images using FAST-MCD method and neural network, *Int. J. Adv. Manuf. Technol.* 129 (3) (2023) 1547–1565.
- [6] S.-K.-S. Fan, C.-Y. Hsu, C.-H. Jen, K.-L. Chen, L.-T. Juan, Defective wafer detection using a denoising autoencoder for semiconductor manufacturing processes, *Adv. Eng. Inf.* 46 (2020), 101166.

- [7] H.-W. Xu, W. Qin, J.-H. Hu, Y.-N. Sun, Y.-L. Lv, J. Zhang, A Copula network deconvolution-based direct correlation disentangling framework for explainable fault detection in semiconductor wafer fabrication, *Adv. Eng. Inf.* 59 (2024), 102272.
- [8] J. Kim, H. Kim, J. Park, K. Mo, P. Kang, Bin2Vec: A better wafer bin map coloring scheme for comprehensible visualization and effective bad wafer classification, *Appl. Sci.* 9 (3) (2019) 597.
- [9] M.H. Hansen, V.N. Nair, D.J. Friedman, Monitoring wafer map data from integrated circuit fabrication processes for spatially clustered defects, *Technometrics* 39 (3) (1997) 241–253.
- [10] D.-H. Lee, J.-K. Yang, C.-H. Lee, K.-J. Kim, A data-driven approach to selection of critical process steps in the semiconductor manufacturing process considering missing and imbalanced data, *J. Manuf. Syst.* 52 (2019) 146–156.
- [11] N. Yu, Q. Xu, H. Wang, Wafer defect pattern recognition and analysis based on convolutional neural network, *IEEE Trans. Semicond. Manuf.* 32 (4) (2019) 566–573.
- [12] H. Kang, S. Kang, A stacking ensemble classifier with handcrafted and convolutional features for wafer map pattern classification, *Comput. Ind.* 129 (2021), 103450.
- [13] W. Shin, H. Kahng, S.B. Kim, Mixup-based classification of mixed-type defect patterns in wafer bin maps, *Comput. Ind. Eng.* 167 (2022), 107996.
- [14] M.G. Kwak, Y.J. Lee, S.B. Kim, SWaCo: safe wafer bin map classification with self-supervised contrastive learning, *IEEE Trans. Semicond. Manuf.* 36 (3) (Aug. 2023) 416–424, <https://doi.org/10.1109/TSM.2023.3280891>.
- [15] M. Saqlain, Q. Abbas, J.Y. Lee, A deep convolutional neural network for wafer defect identification on an imbalanced dataset in semiconductor manufacturing processes, *IEEE Trans. Semicond. Manuf.* 33 (3) (Aug. 2020) 436–444, <https://doi.org/10.1109/TSM.2020.2994357>.
- [16] X. Zheng, S. Zheng, Y. Kong, J. Chen, Recent advances in surface defect inspection of industrial products using deep learning techniques, *Int. J. Adv. Manuf. Technol.* 113 (2021) 35–58.
- [17] Y. Ji, J.-H. Lee, Using GAN to improve CNN performance of wafer map defect type classification: yield enhancement, in: 2020 31st annual SEMI advanced semiconductor manufacturing conference (ASMC), IEEE, 2020, pp. 1–6.
- [18] J. Li, R. Tao, R. Chen, Y. Chen, C. Zhao, X. Huang, Sample-imbalanced wafer map defects classification based on auxiliary classifier denoising diffusion probability model, *Comput. Ind. Eng.* 192 (2024), 110209.
- [19] J. Jang, M. Seo, C.O. Kim, Support weighted ensemble model for open set recognition of wafer map defects, *IEEE Trans. Semicond. Manuf.* 33 (4) (2020) 635–643.
- [20] M. Chu, S. Park, J. Jeong, K. Joo, Y. Lee, J. Kang, Recognition of unknown wafer defect via optimal bin embedding technique, *Int. J. Adv. Manuf. Technol.* 121 (5) (2022) 3439–3451.
- [21] J. Jang, G.T. Lee, Decision fusion approach for detecting unknown wafer bin map patterns based on a deep multitask learning model, *Expert Syst. Appl.* 215 (2023), 119363.
- [22] I. Baek, S.B. Kim, Contrastive deep clustering for detecting new defect patterns in wafer bin maps, *Int. J. Adv. Manuf. Technol.* (2024) 1–11.
- [23] J. Yang, K. Zhou, Y. Li, and Z. Liu, “Generalized out-of-distribution detection: a survey,” *arXiv preprint arXiv:2110.11334*, 2021.
- [24] M.S. Graham, W.H.L. Pinaya, P.-D. Tudosiu, P. Nachev, S. Ourselin, J. Cardoso, Denoising diffusion models for out-of-distribution detection, in: Proceedings of the IEEE/CVF Conference on Computer Vision and Pattern Recognition, 2023, pp. 2947–2956.
- [25] Z. Liu, J. P. Zhou, Y. Wang, and K. Q. Weinberger, Unsupervised out-of-distribution detection with diffusion inpainting, in: International Conference on Machine Learning, PMLR, 2023, pp. 22528–22538.
- [26] M.-J. Wu, J.-S.-R. Jang, J.-L. Chen, Wafer map failure pattern recognition and similarity ranking for large-scale data sets, *IEEE Trans. Semicond. Manuf.* 28 (1) (2014) 1–12.
- [27] J. Wang, C. Xu, Z. Yang, J. Zhang, X. Li, Deformable convolutional networks for efficient mixed-type wafer defect pattern recognition, *IEEE Trans. Semicond. Manuf.* 33 (4) (2020) 587–596.
- [28] C.M. Bishop, Novelty detection and neural network validation, *IEE Proceedings-Vision, Image and Signal Processing* 141 (4) (1994) 217–222.
- [29] H. Choi, E. Jang, A. A. Alemi, “Waic, but why? generative ensembles for robust anomaly detection,” *arXiv preprint arXiv:1810.01392*, 2018.
- [30] J. Ren, et al., Likelihood ratios for out-of-distribution detection, *Adv. Neural Inf. Process Syst.* 32 (2019).
- [31] P. Kirichenko, P. Izmailov, A.G. Wilson, Why normalizing flows fail to detect out-of-distribution data, *Adv. Neural Inf. Process Syst.* 33 (2020) 20578–20589.
- [32] D. Gong et al., Memorizing normality to detect anomaly: memory-augmented deep autoencoder for unsupervised anomaly detection, in: Proceedings of the IEEE/CVF international conference on computer vision, 2019, pp. 1705–1714.
- [33] S. Choi, H. Lee, H. Lee, M. Lee, Projection regret: reducing background bias for novelty detection via diffusion models, *Adv. Neural Inf. Process Syst.* 36 (2024).
- [34] A. Radford et al., Learning transferable visual models from natural language supervision, in: International conference on machine learning, PMLR, 2021, pp. 8748–8763.
- [35] A. Ramesh et al., Zero-shot text-to-image generation, in: International conference on machine learning, PMLR, 2021, pp. 8821–8831.
- [36] C. Saharia et al., Palette: Image-to-image diffusion models, in: ACM SIGGRAPH 2022 conference proceedings, 2022, pp. 1–10.
- [37] J. Ho, A. Jain, P. Abbeel, Denoising diffusion probabilistic models, *Adv. Neural Inf. Process Syst.* 33 (2020) 6840–6851.
- [38] R. Zhang, P. Isola, A. A. Efros, E. Shechtman, O. Wang, The unreasonable effectiveness of deep features as a perceptual metric, in: Proceedings of the IEEE conference on computer vision and pattern recognition, 2018, pp. 586–595.
- [39] T. Schlegl, P. Seeböck, S. M. Waldstein, U. Schmidt-Erfurth, and G. Langs, Unsupervised anomaly detection with generative adversarial networks to guide marker discovery, in: International conference on information processing in medical imaging, Springer, 2017, pp. 146–157.
- [40] R. Rombach, A. Blattmann, D. Lorenz, P. Esser, B. Ommer, High-resolution image synthesis with latent diffusion models, in: Proceedings of the IEEE/CVF conference on computer vision and pattern recognition, 2022, pp. 10684–10695.
- [41] K. He, X. Zhang, S. Ren, J. Sun, Deep residual learning for image recognition, in: Proceedings of the IEEE conference on computer vision and pattern recognition, 2016, pp. 770–778.
- [42] D.P. Kingma, J. Ba, “Adam: A method for stochastic optimization,” 2014, *arXiv preprint arXiv:1412.6980*.
- [43] M.S. Graham et al., Unsupervised 3d out-of-distribution detection with latent diffusion models, in: International Conference on Medical Image Computing and Computer-Assisted Intervention, Springer, 2023, pp. 446–456.
- [44] H. Kahng, S.B. Kim, Self-supervised representation learning for wafer bin map defect pattern classification, *IEEE Trans. Semicond. Manuf.* 34 (1) (Feb. 2021) 74–86, <https://doi.org/10.1109/TSM.2020.3038165>.
- [45] Y. Song, P. Dhariwal, M. Chen, I. Sutskever, Consistency models, in: Proceedings of the 40th International Conference on Machine Learning, 2023, pp. 32211–32252.